Dalton Transactions

Accepted Manuscript

ROYAL SOCIETY OF CHEMISTRY

www.rsc.org/dalton

Assessment of density functionals and paucity of non-covalent interactions in aminoylyne complexes of molybdenum and tungsten [(η^5-C_5H_5)$(CO)_2$M≡EN($SiMe_3$)(R)] (E = Si, Ge, Sn, Pb): A dispersion-corrected DFT study

Krishna K. Pandey,*[a] Pankaj Patidar, Pankaj K. Bariya, Sunil K. Patidar and Ravi Vishwakarma

[a]*School of Chemical Sciences, Devi Ahilya University Indore, Khandwa Road Campus, Indore 452001, India*

ABSTRACT

Electronic, molecular structure and bonding energy analysis of the metal-aminosilylyne, -aminogermylyne, -aminostannylyne and -aminoplumbylyne complexes [(η^5-C_5H_5)$(CO)_2$M≡EN($SiMe_3$)(Ph)] (M = Mo, W) and [(η^5-C_5H_5)$(CO)_2$Mo≡GeN($SiMe_3$)(Mes)] have been investigated at DFT, DFT-D3 and DFT-D3(BJ) level using BP86, PBE, PW91, RPBE, TPSS and M06-L functionals. Performance of metaGGA functionals for the geometries of aminoylyne complexes is better than GGA functionals. Significant dispersion interactions between O---H, E---C(O) and E---H pairs are appeared in the dispersion-corrected geometries. The non-covalent distances of these interaction follow the order DFT > DFT-D3(BJ) > DFT-D3. The values of Nalewajski-Mrozek bond orders (1.22 – 1.52) and Pauling bond order (2.23 – 2.59) of the optimized structures at BP86/TZ2P indicate the presence of a multiple bond between metal and E atoms. The overall electronic charges transfer from transition-metal fragments to ligand. The topological analysis based on QTAIM has been performed to determine the analogy of non-covalent interactions. The strength of M≡EN($SiMe_3$)(R) bonds has been evaluated by energy decomposition analysis. The electrostatic interactions are almost equal to orbital interactions. The M ← E σ-donation is smaller than the M → E π-back donation. Upon going from E = Si to E = Pb, the M-E bond orders decrease as Si > Ge > Sn > Pb, consistent with the observed geometry trends. The M-E uncorrected bond dissociation energies vary with the density functionals as RPBE < BP86 < PBE < TPSS < PW91. The largest DFT-D3 dispersion corrections to the BDEs corresponds to the BP86 functional, ranging between 5.6−8.1 kcal/mol, which are smaller than the DFT-D3(BJ) dispersion corrections (10.1−12.0 kcal/mol). The aryl substituents on nitrogen have insignificant effect on M-E-N bending. The bending of the M-E-N bond angle has been discussed in terms of Jahn-Teller distortion. The larger noncovalent interaction

and smaller absolute values of ΔE(HOMO-LUMO) with M06-L functional are responsible for lowering the M-E-N bond angle.

Keywords: Dispersion, Bonding, Triple bond, Molybdenum, Tungsten, QTAIM

Tel.: 00 91 731 2460208; Fax: 00 91 731 2762342
*To whom correspondence should be addressed. E-mail: kkpandey.schem@dauniv.ac.in (KKP)

1. Introduction

Issues regarding the electronic structure and bonding analysis in transition metal-silylyne, -germylyne, -stannylyne and plumbylyne complexes [$L_nM{\equiv}ER$], have been a pivotal subject since the first structurally characterized molybdenum-germylyne complex [$(\eta^5\text{-}C_5H_5)(CO)_2Mo{\equiv}GeR$] (R = 2,6-(2,4,6-$Me_3C_6H_2)_2C_6H_3$), reported by Simon and Power in 1996.[1] In the intervening seventeen years, the chemistry of the transition metal-ylyne complexes has blossomed leading to an in-depth understanding of synthesis, structure, bonding and reactivity.[2] So far a number of structurally characterized terminal transition metal-ylyne complexes have been reported.[3-23] These complexes are largely limited to chromium, molybdenum and tungsten and contain bulky aryl or alkyl substituents at E atoms.[4-20] However, representative examples of triply bonded complexes of manganese, rhenium and osmium have also been reported rather recently.[21-23] All the complexes show essentially linear M-E-C(R) linkages. Jones and coworkers reported the first representative aminogermylyne complex of molybdenum [$(\eta^5\text{-}C_5H_5)(CO)_2Mo{\equiv}GeN(SiMe_3)(Ar^*)$] (Ar* = $C_6H_2\{C(H)Ph_2\}_2$Me-2,6,4), having a di-substituted amino group at germanium instead of alkyl group.[24] The Mo≡Ge-N angle (155.81(8)°) in this complex is significantly distorted from linearity.

The electronic structure and bonding situation of transition metal-ylyne (M-ER) complexes of chromium, molybdenum, tungsten and iron have been investigated in theoretical studies[25-31] including the differences between the chemical bonding situation of metal-ylynes and metalloylenes.[25,28] In a recent publication, the nature of M-Ge bonds in aminogermylene complexes of chromium, molybdenum and tungsten complexes have also been reported.[32] However, the M≡E-N bonding nature in the aminoylyne complexes as a function of heavier group 14 elements still remain to be explored. The quantum-chemical calculations of the complex [$(\eta^5\text{-}C_5H_5)(CO)_2Mo{\equiv}GeN(SiMe_3)(Ar^*)$] has been carried out at B3LYP/6-311G(d)/ LANL2DZ level

along with synthetic details.[24] The authors have suggested that the distortion in Mo≡Ge-N angle may arises due to the buttressing between metal fragment and substituents of amido group as well as contribution of $Mo^{(-)}$=Ge=$N^{(+)}$ canonical form to the Mo≡Ge-N bonding.[24] However, both the effects would most favorable in linear arrangement and therefore, do not explain the appropriate reasons of Mo-Ge-N bending. A more detailed understanding of the structure and bonding in transition metal-aminoylyne complexes is utmost important, particularly for the synthesis of silicon, tin and lead analogues and to explain the M-E-N bending.

The non-covalent interactions play a crucial role for accurate prediction of thermodynamic parameters of metal-ligand bonds.[33] As the systems under study become larger, the non-covalent interactions (NCIs) tend to become more important. Unfortunately, the standard density functionals theory (DFT) calculations face difficulty to correctly describe the NCIs.[34] In recent years, a plethora of schemes has been proposed to treat dispersion interactions within DFT.[35-40] Among them, Grimme's atom pair wise dispersion corrections with zero damping, DFT-D3,[41] and with Becke-Johnson damping,[42] DFT-D3(BJ),[43] are convenient and widely used approaches to obtain dispersion contributions in molecular systems.[44] However, the efficiency of computational calculations is strongly depends on the selection of right density functional for the individual problem.[45]

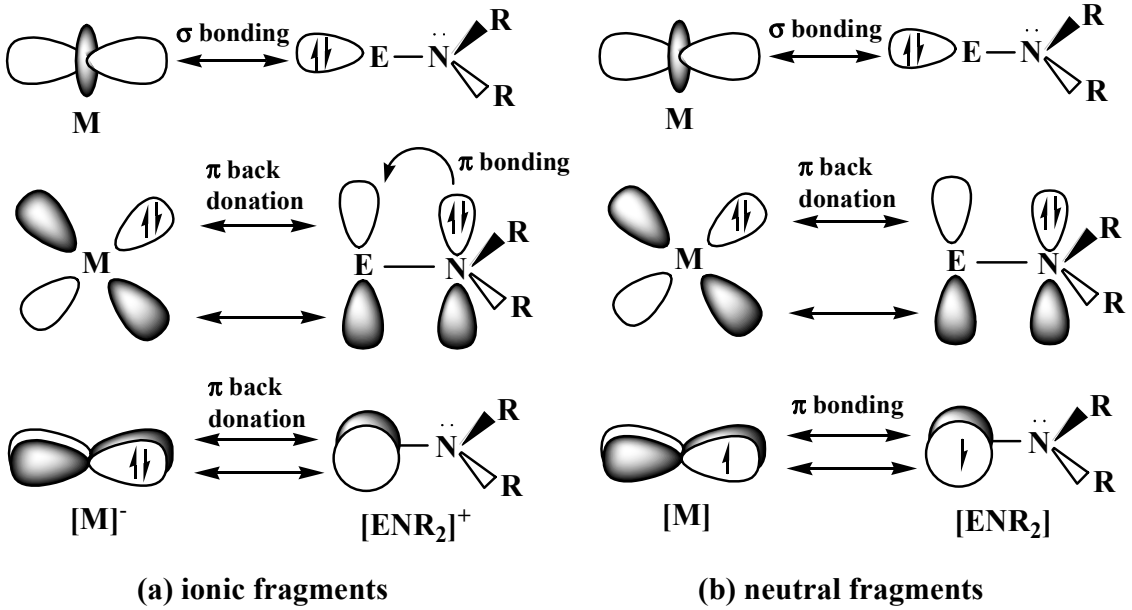

Fig. 1 Schematic representation of the possible orbital interactions between closed shell metal fragments $[(\eta^5\text{-}C_5H_5)(CO)_2M]^-$ and ligands ENRR′ in transition metal-aminoylyne complexes.

In the present paper, we present a comprehensive study on the geometries and bonding nature of nine complexes with linear M≡E-N linkages $[(\eta^5\text{-}C_5H_5)(CO)_2M{\equiv}EN(SiMe_3)(Ph)]$ (M = Mo: **I**, E = Si; **II**, E = Ge; **III**, E = Sn; **IV**, E = Pb; M = W: **V**, E = Si; **VI**, E = Ge; **VII**, E = Sn; **VIII**, E = Pb) and $[(\eta^5\text{-}C_5H_5)(CO)_2Mo{\equiv}GeN(SiMe_3)(Mes)]$ (**IX**) using different density functionals BP86, PBE, RPBE, PW91, TPSS and M06-L. The geometries of the actual complex $[(\eta^5\text{-}C_5H_5)(CO)_2Mo{\equiv}GeN(SiMe_3)(Ar^*)]$ (**X**) with no simplification in the aryl group have also been optimized using different density functionals. The key issues regarding this study are (i) to determine the optimized structures and to analyze the nature of the M≡E-N bonds in metal-silylyne, -germylyne, -stannylyne and –plumbylyne complexes, (ii) to determine and describe the London dispersion interactions in the studied complexes, (iii) to evaluate the contribution of dispersion interactions to the M≡E-N bonding strength, and (iv) to investigate the relative strength of the electrostatic and covalent contributions as well as the contributions of the M←E σ-bonding, and M→E π back-

bonding to the total M≡E-N bonding energy. All the factors are addressed as a function of transition metals as well as a function of E (Si, Ge, Sn, Pb). The presence of covalent and non-covalent interactions is justified by topological analysis based on quantum theory of atoms in molecules (QTAIM) of Bader. The effects of dispersion interactions on molecular geometries as well as on M≡E binding energies have been evaluated utilizing DFT-D3 and DFT-D3(BJ) methods. We report the energy decomposition analysis (EDA) of the M≡EN($SiMe_3$)(R) bonds, which gives the energies that are associated with the M←E σ-bonding, and M→E π back-bonding (see Fig. 1for schematic presentation of the M≡ENRR′ bonds).

2. Computational methods

To examine the effects of density functionals on geometry of the aminoylyne complexes [(η^5-C_5H_5)$(CO)_2$M≡EN($SiMe_3$)(Ph)] (M = Mo, W) (**I** – **VIII**), [(η^5-C_5H_5)$(CO)_2$Mo≡GeN($SiMe_3$)(Mes)] (**IX**) and [(η^5-C_5H_5)$(CO)_2$Mo≡GeN($SiMe_3$)(Ar*)] (**X**) we employed four generalized gradient approximation functionals (GGAs) BP86,[46] PBE,[47] RPBE,[48] PW91[49] and two meta-GGA functionals TPSS[50] and M06-L[51] in the geometry optimization. Grimme's atom pair wise dispersion correction methods, *i.e.* DFT-D3 with zero damping function,[41] and DFT-D3(BJ)[43] with BJ damping function, were used to account the dispersion interactions. Scalar relativistic effects have been considered using the ZORA formalism.[52,53] Uncontracted Slater-type orbitals (STOs) were used as basis functions for the SCF calculations.[54] Triple-ζ basis sets augmented by two sets of polarization function have been used for all the elements. The $(1s)^2$ core electrons of the carbon, nitrogen, oxygen, $(1s2s2p)^{10}$ core electrons of silicon, $(1s2s2p3s3p3d)^{28}$ core electrons of germanium and molybdenum, $(1s2s2p3s3p3d4s4p)^{36}$ core electrons of tin and $(1s2s2p3s3p3d4s4p4d)^{46}$ core electrons of lead and tungsten were treated by the frozen-core approximation.[55] An auxiliary set of s, p, d, f and g STOs was used to fit the molecular densities and to present the coulomb and exchange potentials accurately

in each SCF cycle.[54] The calculations were carried out using the program package ADF-2013.01.[56] The electronic structures of the complexes (**I-IX**) were examined by Nalewajski-Mrozek (N-M) bond orders,[57] Voronoi deformation density (VDD) charges,[58] Hirshfeld charges[59] and NHO analysis.[60] The non-covalent interactions have been determined by quantum theory of atoms in molecule (QTAIM)[61] calculations in terms of bond critical points. All MO pictures were made by using the MOLDEN program.[62]

The bonding interactions between metal fragment $[(\eta^5\text{-}C_5H_5)(CO)_2M]^-$ or $[(\eta^5\text{-}C_5H_5)(CO)_2M]$ (M = Mo, W) and ligand fragments $[EN(SiMe_3)(R)]^+$ or $[EN(SiMe_3)(R)]$ (R = Ph, Mes) have been analyzed in C_s symmetry at DFT/BP86 level using the energy decomposition scheme of the program package ADF,[63] which is based on the work by Morokuma[64] and Ziegler and Rauk.[65,66] The bond dissociation energy (BDE) between the fragments is partitioned into several contributions which can be identified as physically meaningful quantities. First, ΔE is separated into two major components ΔE_{int} and ΔE_{prep}:

$$\Delta E = \Delta E_{int} + \Delta E_{prep} \qquad (1)$$

ΔE_{prep} is the energy, which is necessary to promote the fragments from their equilibrium geometry and electronic ground state to the geometry, and electronic state, which they have in the molecule. The instantaneous interaction energy ΔE_{int} is the focus of the bonding analysis and can be decomposed into three components:

$$\Delta E_{int} = \Delta E_{elstat} + \Delta E_{Pauli} + \Delta E_{orb} \qquad (2)$$

The term ΔE_{elstat} gives the electrostatic interaction energy between the fragments which are calculated with a frozen density distribution in the geometry of the complex. The term ΔE_{Pauli}, which

is called exchange repulsion or Pauli repulsion, takes into account the destabilizing two-orbital three- or four-electron interactions between occupied orbitals of both fragments. ΔE_{Pauli} is calculated by enforcing the Kohn-Sham determinant of the molecule, which results from superimposing both fragments, to obey the Pauli principle through antisymmetrization and renormalization. The last term ΔE_{orb} in equation 2 gives the stabilizing orbital interactions between occupied and virtual orbitals of the two fragments. ΔE_{orb} can be further partitioned into contributions by the orbitals that belong to different irreducible representations of the point group of the system. It has been shown that the results of EDA give a quantitative insight into the nature of metal-ligand interactions.[67-69]

3. Results and discussion

3.1. Geometries. The important geometrical parameters of the ten aminoylyne complexes, **I** – **X** calculated using the density functional BP86, PW91, PBE, RPBE, TPSS and M06-L are presented in Table 1. Fig. 2 shows the BP86/TZ2P optimized geometries of the aminogermylyne complexes [(η^5-C_5H_5)$(CO)_2$M≡GeN($SiMe_3$)(Ph)] (M = Mo, W) and [(η^5-C_5H_5)$(CO)_2$Mo≡GeN($SiMe_3$)(Mes)] (**IX**). The structures of silylyne, stannylyne and plumbylyne complexes are very similar to those presented in this figure and are therefore not included. The optimized geometries of the aminogermylyne complexes [(η^5-C_5H_5)$(CO)_2$Mo≡GeN($SiMe_3$)(R)] (R = Ph, Mes, Ar*) are in good agreement with the experimental values reported for the complex [(η^5-C_5H_5)$(CO)_2$Mo≡Ge($SiMe_3$)(Ar*)][24] (Table 1). As can be seen in Table 1, the different density functionals provide almost similar geometrical parameters for particular aminoylyne complex. However, a keen comparison of geometries reveals that the performance of the meta-GGA functionals (TPSS and M06-L) for the geometries of the studied complexes is slightly better than the GGA functionals. The M06-L meta-GGA functional estimates M-E-N bond angle more accurate, close to the experimental value. The RPBE functional relatively overestimate the geometrical data as compare to the other employed GGA functionals.

Table 1

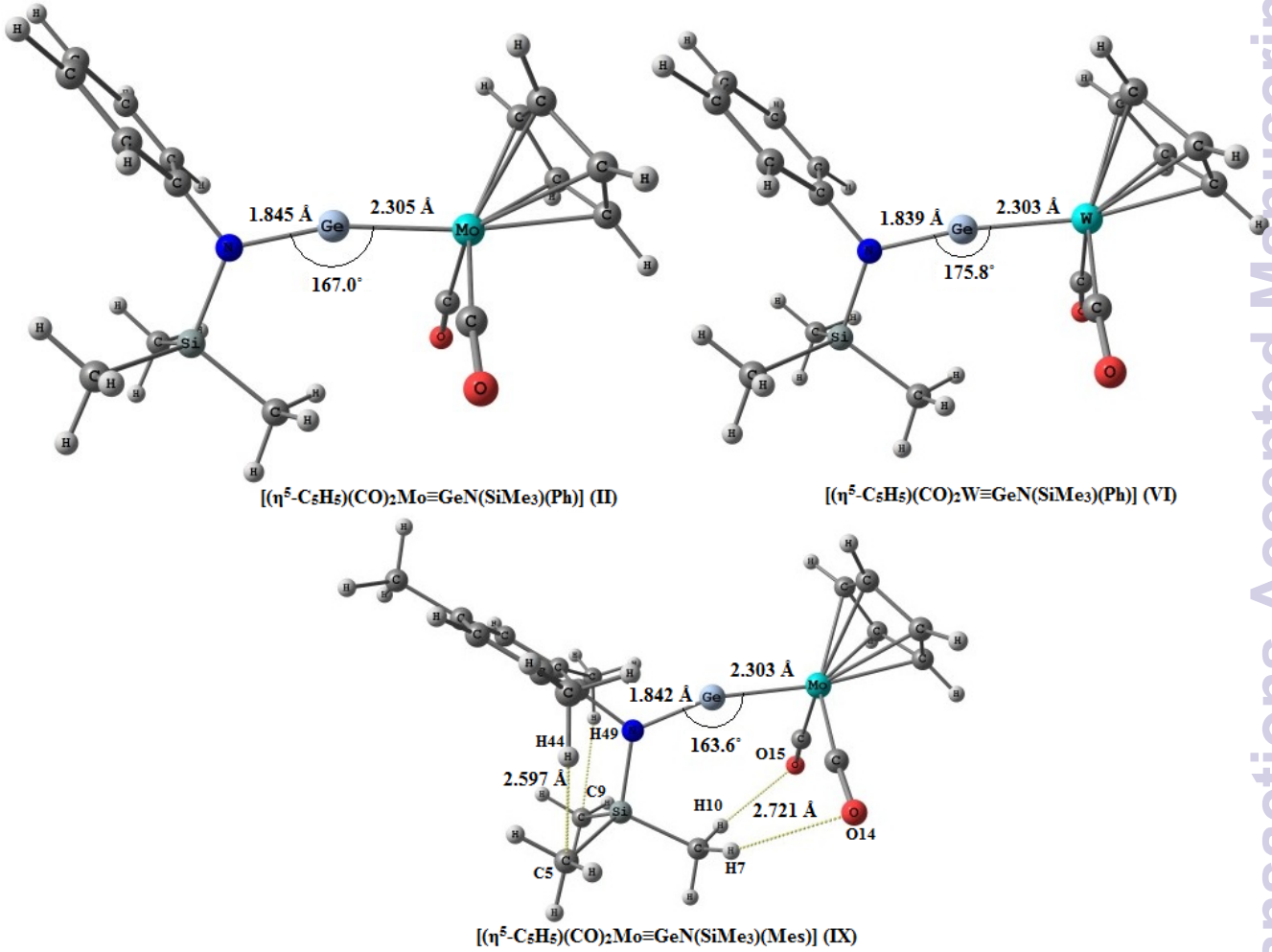

Fig. 2 BP86/TZ2P optimized structures of the aminogermylyne complexes [(η^5-C_5H_5)$(CO)_2$M≡GeN($SiMe_3$)(Ph)] (**II**, M=Mo; **VI**, M = W) and, BP86-D3 optimized geometry of [(η^5-C_5H_5)$(CO)_2$M≡GeN($SiMe_3$)(Mes)] (**IX**).

The M-E bond distances in the complexes, **I – X** are significantly shorter than those expected from single bond covalent radii predictions (Mo-Si = 2.54 Å, Mo-Ge = 2.59 Å, Mo-Sn = 2.78 Å, Mo-Pb = 2.82 Å; W-Si = 2.53 Å, W-Ge = 2.58 Å, W-Sn = 2.77 Å, W-Pb = 2.81 Å),[70] suggesting the

presence of multiple bond characters between M and E. The M-E bond distances increase in periodic trend, upon descending in group 14, while remains almost equal on going from molybdenum to tungsten (although covalent radii of Mo and W differs by 0.1 Å). It is important to note that the M≡E bond distances (with BP86/TZ2P) in the aminoylyne complexes are longer than those in the complexes $[(\eta^5\text{-}C_5H_5)(CO)_2M{\equiv}EMe]$, for example, 2.247 Å > 2.229 Å (for Mo≡Si), 2.305 Å > 2.286 Å (for Mo≡Ge), 2.503 Å > 2.482 Å (for Mo≡Sn) and 2.561 Å > 2.522 Å (for Mo≡Pb). The lengthening of M-E bonds in the complexes **I** - **X** is accompanied with the formation of an E-N π-bonding interaction. As depicted in Fig. 1, the nitrogen can donate π-electron density to the heavier E element which results in E-N multiple bonding characters and reduces the π-acidity of ENR_2 ligands. The optimized Si-N, Ge-N, Sn-N and Pb-N bond distances in the complexes **I** - **X** (Table 1) are shorter than those expected for single bonds based on covalent radii (Si-N = 1.87 Å, Ge-N = 1.92 Å, Sn-N = 2.11 Å, Pb-N = 2.15 Å).[70] The M-E-N bond angles are slightly bent in the all studied complexes, ranging from 150.8º to 177.4º. The computed M-E-N angles of the tungsten complexes are much closer to linearity than their molybdenum congeners. It has been stated earlier that the M-E-N bending in these complexes is due to the steric bulk of the amido group.[24] However, interactions that arises from the amido group and concerning to the M-E-N bending in aminoylyne complexes have not been described clearly. The PES associated with M-E-N bending in tungsten complexes $[(\eta^5\text{-}C_5H_5)(CO)_2W{\equiv}EN(SiMe_3)(Ph)]$ are presented in Fig. S1 (Supporting Information).

Fig. 3 shows the noncovalent interaction in complexes $[(\eta^5\text{-}C_5H_5)(CO)_2Mo{\equiv}GeN(SiMe_3)(Ph)]$ (**II**) and $[(\eta^5\text{-}C_5H_5)(CO)_2Mo{\equiv}GeN(SiMe_3)(Mes)]$(**IX**). From Fig. 3 we observed that (i) the aryl groups (Ph, Mes) do not have noncovalent interaction with Ge atom, (ii) Ortho methyl group hydrogen has dispersion interaction with nitrogen and not with Ge, (iii) Ge---$C(SiMe_3)$ and $H(SiMe_3)$---O(CO) noncovalent interaction are observed and (iv) Ge---$C(SiMe_3)$ noncovalent

interaction is more in complex (**IX**) than in complex (**II**). Thus, the aryl substituents on nitrogen have insignificant effect on M-E-N bending.

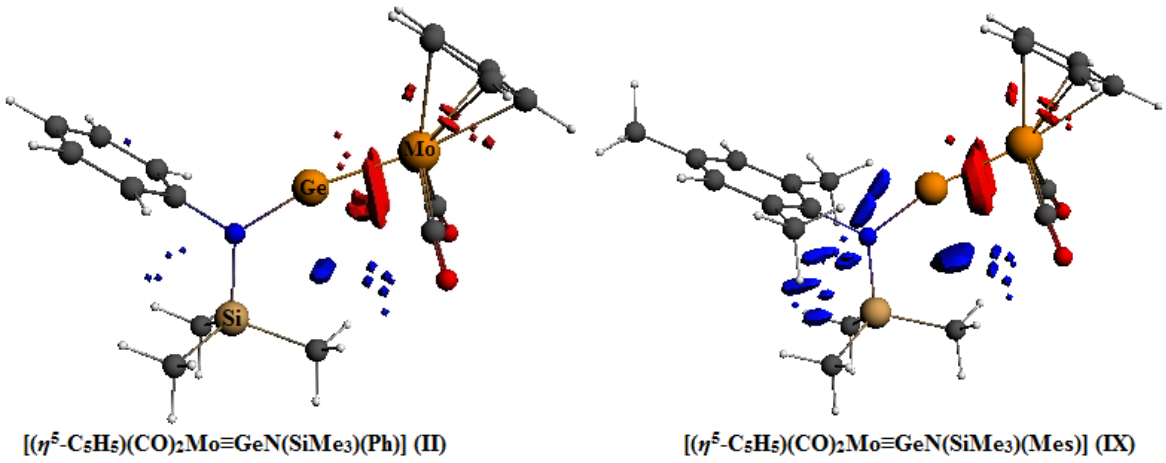

Fig. 3 The noncovalent interaction in complexes [(η^5-C_5H_5)$(CO)_2$Mo≡GeN$(SiMe_3)$(Ph)] (**II**) and [(η^5-C_5H_5)$(CO)_2$Mo≡GeN$(SiMe_3)$(Mes)](**IX**).

Fig. 4 depicts the noncovalent interaction in complex [(η^5-C_5H_5)$(CO)_2$W≡SnN$(SiMe_3)$(Ph)] (**VII**) with BP86 and M06-L functionals. As seen in Fig. 4, the Sn---C$(SiMe_3)$ noncovalent interaction with M06-L functional is significantly larger than that with BP86 functional without dispersion correction. The larger noncovalent interaction with M06-L functional is responsible for lowering the W-Sn-N bond angle.

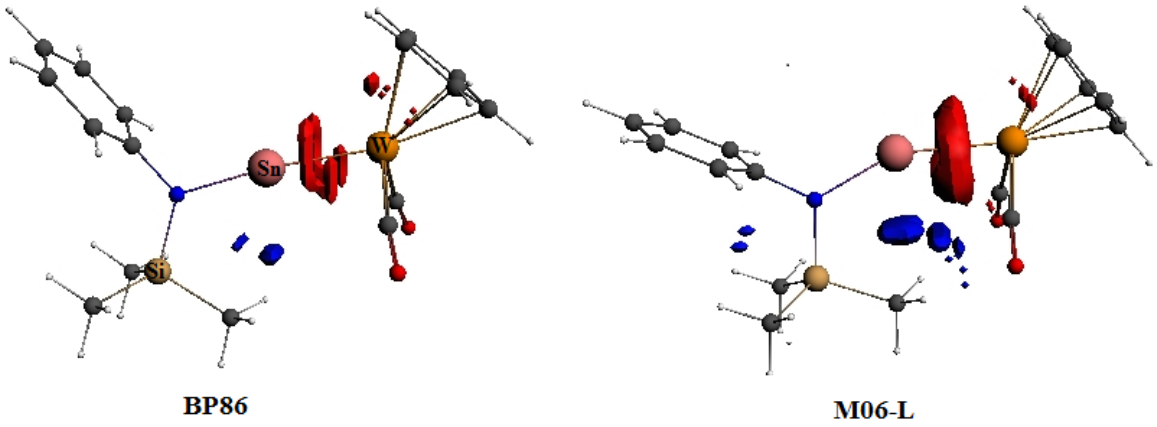

Fig. 4 The noncovalent interaction in complex [(η^5-C_5H_5)$(CO)_2$W≡SnN($SiMe_3$)(Ph)] (**VII**) with density functional BP86 and M06-L.

The bending of the M-E-N bond angle has been discussed in terms of Jahn-Teller distortion.[71] As the absolute value of ΔE (HOMO - LUMO) decreases, the M-E-N angle decreases due to relatively greater mixing of HOMO and LUMO. Variation of W-Sn-N bond angle in complex [(η^5-C_5H_5)$(CO)_2$W≡SnN($SiMe_3$)(Ph)] (**VII**) with ΔE for density functionals BP86, PW91, PBE, RPBE and M06-L is presented in Fig. 5. The data are given in Table S1 (Supporting Information), it could be concluded that as the absolute value of ΔE decreases, the W-Sn-N angle also decreases due to relatively greater mixing of HOMO and LUMO. The absolute value of ΔE for M06-L functional (2.072) is significantly smaller than that for BP86 functional (2.209). The results are consistent with W-Sn-N bond angles (155.1º with M06-L) and (173.4º with BP86).

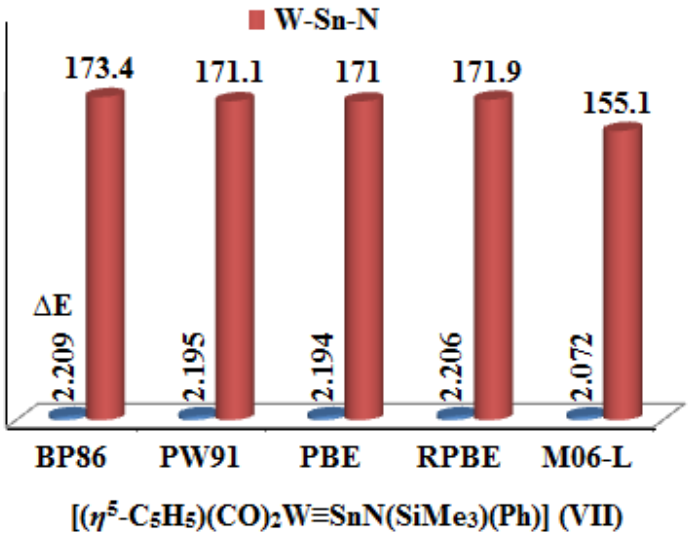

Fig. 5 The variation of W-Sn-N bond angle with ΔE (HOMO-LUMO) in complex [(η^5-C_5H_5)$(CO)_2$W≡SnN($SiMe_3$)(Ph)](**VII**).

To determine the effect of non-covalent interactions on molecular geometry, we have optimized the complex [(η^5-C_5H_5)$(CO)_2$Mo≡GeN($SiMe_3$)(Mes)] by employing the Grimme's dispersion corrections, DFT-D3 and DFT-D3(BJ), to density functionals BP86, PBE and TPSS . The important results are presented in Table 2.

Table 2

The M≡E and E-N bond distances decrease, albeit minor, in the order DFT > DFT-D3 > DFT-D3(BJ). The important non-covalent distances Ge---C(O), C(5/9)---H(44/49) and O(14/15)---H(7/10) (See Fig. 2 for notation) shows significant variations with the inclusion of dispersion. Note that the dispersion-corrected O---H distances of **IX** are in the range of typical O---H hydrogen bonding (2.6 Å -3.2 Å) and could be treated as hydrogen bonding (Table 2). The strength of O---H as well as E---C(O) interactions increases in the order DFT < DFT-D3(BJ) < DFT-D3. We expect that these non-

covalent interactions between metal fragment and aminoylyne ligands, especially O---H interactions, might be responsible for the bending of M-E-N bond angles.

3.2. Bonding analysis of M≡E bonds. The electronic pictures of the Mo≡ENR_2 bonding in the complexes [(η^5-C_5H_5)$(CO)_2$Mo≡EN($SiMe_3$)(Ph)] (**I** – **IV**) can be visualized in Fig. 6. The HOMO (HOMO-1 for silylyne complex) gives a pictorial description of the Mo-E out-of-plane π-bonding orbital, while HOMO-2 is in-plane π-bonding orbital. One can observe that the π-bonds are polarized towards metal centre. It is also important that the M≡E π-bonding orbitals carry a partial contribution from C(O) electron densities, which may arises due to the E---C(O) interactions. On going from E = Si to E = Pb, the continuous increase in the size of the p_π orbitals decreases the overlap and, therefore, weakens the Mo-E π-bonds. It is worth noting that the Fischer-type model of bonding is well suited. The HOMO-10 is a Mo-E σ-bonding orbital, which is polarized toward the ligand EN($SiMe_3$)(Ph). On going from E = Si to E = Pb, the sp_σ orbital becomes less directional and more diffuse and a poor charge transfer is observed. Molecular orbitals shown in Fig. 6c are predominantly E-N π-bonding orbitals. The π-bonding contribution to E-N bonds also diminishes on going from Si to Pb.

Table 3

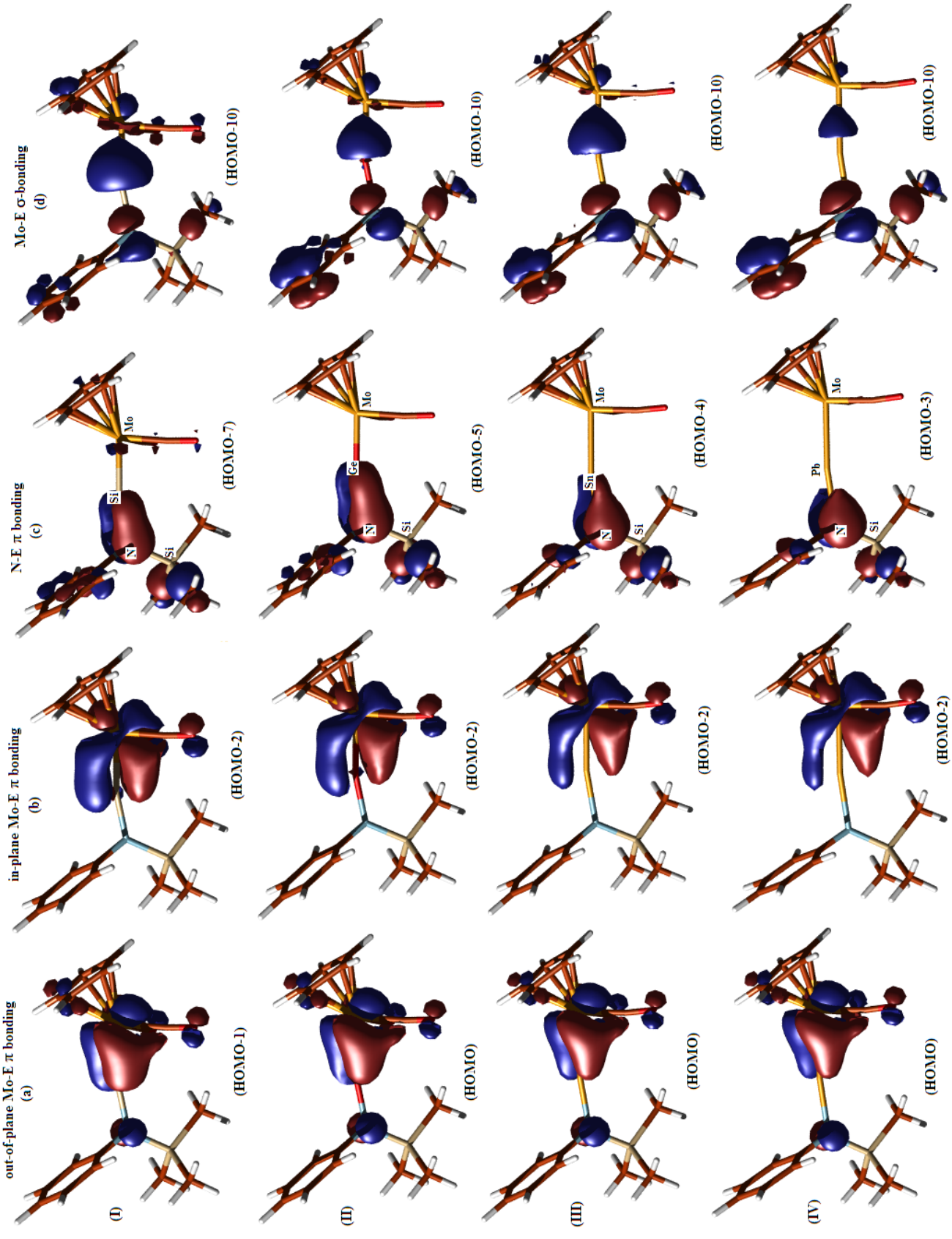

Fig. 6 Plots of some relevant molecular orbitals of the molybdenum-ylyne complexes $[(\eta^5\text{-}C_5H_5)(CO)_2Mo{\equiv}EN(SiMe_3)(Ph)]$ (E = Si, **I**; Ge, **II**; Sn, **III**; Pb, **IV**) at BP86/TZ2P level.

The pictorial representation of the molecular orbital shall now be complemented with results of the electronic structure analysis for the complexes **I** - **X**. A detailed analysis of the electronic structure of the complexes **I** - **X** is obtained from Nalewajski-Mrozek (N-M) bond orders,[57] Voronoi deformation densities (VDD) charges,[58] and the Hirshfeld charges,[59] which is presented in Table 3. The Nalewajski-Mrozek (N-M) bond orders (1.22 – 1.52) indicate a multiple bond nature of M-E bond. It has been noted previously the N-M bond orders are usually lower than classical integer values.[72] However, the Pauling bond order[73] of the optimized M-E bond distances in these complexes are 2.59 (**I**), 2.52 (**II**), 2.45 (**III**), 2.32 (**IV**), 2.46 (**V**), 2.45 (**VI**), 2.38 (**VII**), 2.23 (**VIII**), 2.49 (**IX**), 2.44 (**X**). Thus, the N-M and Pauling bond orders indicate multiple bond character between M and E in the complexes **I** - **X**. Upon going from E = Si to E = Pb, the M-E bond orders decrease as Si > Ge > Sn > Pb, consistent with the observed geometry trends. The N-M bond orders for E-N bonds (0.93 – 1.16) in the complexes (**I** - **X**) also indicate E-N multiple bond character. E-N bond orders in free ligands are: 1.60 in $[SiN(SiMe_3)(Ph)]^+$, 1.55 in $[GeN(SiMe_3)(Ph)]^+$, 1.37 in $[SnN(SiMe_3)(Ph)]^+$, 1.31 in $[PbN(SiMe_3)(Ph)]^+$, 1.51 in $[GeN(SiMe_3)(Mes)]^+$ and 1.50 in $[GeN(SiMe_3)(Ar^*)]^+$. Upon coordination, the E-N bond orders are calculated to be reduced. The transition metal atoms (0.23-0.07) and heavier group 14 elements (0.38-0.19) always carries a positive Hirshfeld charge. The nitrogen atom bears a significant negative charge in all the studied complexes. The large charge separation between the interacting fragments results in significant electrostatic interactions. As seen in Table 3, the VDD and Hirshfeld charges give almost similar values. The negative charges on the metal fragments $[(\eta^5\text{-}C_5H_5)(CO)_2M]$ and positive charges on the ligand fragments $[EN(SiMe_3)(Ph)]$, suggest the donor-acceptor bonding pattern, considering an ionic fragmentation scheme (as shown in Fig.1) should be more appropriate.

A more definitive picture of M≡E bonding is obtained through an NHO analysis of the Kohn-Sham orbitals. The important characteristics of the M≡E bonds are listed in Table S2. The M≡E σ-bonds are well occupied (> 1.852*e*) and are polarized towards the E atoms. In all complexes (**I – IX**), the polarization of σ-bonding orbitals sharply increases for the plumbylidyne complexes, perhaps due to relativistic effects of Pb. The s character contribution of E atom to the M-E σ-bonds increases from silicon to lead. On the other hand, both the M≡E π-bonding orbitals are polarized towards the transition metal center in all complexes and polarization successively increases in the manner as Si < Ge < Sn < Pb. The E-N σ-bonds are markedly polarized towards the more electronegative nitrogen atom. One important difference in M≡E bonding of $[(\eta^5\text{-}C_5H_5)(CO)_2M{\equiv}ER]$ and $[(\eta^5\text{-}C_5H_5)(CO)_2M{\equiv}EN(SiMe_3)(R)]$ is that the M-E σ-bonds in former complexes are composed of sd^n hybridized orbital at transition metal,[28] while in latter complexes, significantly larger contribution of p characters in σ-bonding orbitals is observed.

To justify the existence of non-covalent interactions in the aminoylyne complexes, we perform the QTAIM analysis (quantum theory of atoms in molecule) of the complex **IX** at DFT-D3/BP86 level. The presence of non-covalent interactions has been determined by the [3,-1] bond critical points (BCPs). Bond paths and associated critical points, Plot of reduced density gradient (RDG) at low density for non-covalent interactions and molecular orbitals showing O---H and C---H interactions are presented in Fig.7. The electron distributions, ρ(r) and associated Laplician, $\nabla^2\rho$, at the important bond critical points (BCPs) and ring critical points (RCPs) are given in Table S3 in Supporting Information. It is known that value of $\rho_{(BCP)} < 0.1$ a.u. and relatively small, positive values of Laplacian, $\nabla^2\rho$, is expected for closed-shell (*i.e.*, predominantly non-covalent) interactions.[74] Therefore, the BCPs for O---H and C---H interactions can be are characterized as O---H hydrogen bonding and C---H van der Waals interactions. The electron density at the BCPs reflects the strength

of the concerning interactions. Note that the $\rho_{(BCP)}$ = 0.0841 a.u. of Mo-Ge is significantly larger than the $\rho_{(BCP)}$ of O---H and C---H (0.0057 a.u. and 0.0098 a.u., respectively). Our lower values of electron density at BCP for CH---O interaction (0.0057 a.u) suggest the non-covalent interactions. The higher values have been observed in case of (CH---O) hydrogen bond.[75] In addition, four non-structural rings are formed due to the above mentioned NCIs (Fig.7). The ring critical points (RCPs), accompanied with these rings, are well-placed inside the ring and marked with circles. The electron density at RCPs are comparable with the $\rho_{(BCP)}$ values of the O---H interactions (Table S3). All the interactions characterized by topological properties at the BCPs and RCPs contribute to the overall stability of the studied aminoylyne complexes. However, the BCPs and RCPs, which are generated by the close contacts of O---H, enhance the bonding interactions between transition metal fragments [(η^5-C_5H_5)$(CO)_2$M] and ligands [EN($SiMe_3$)(R)] and results slight distortion in angle M≡E-N from linearity.

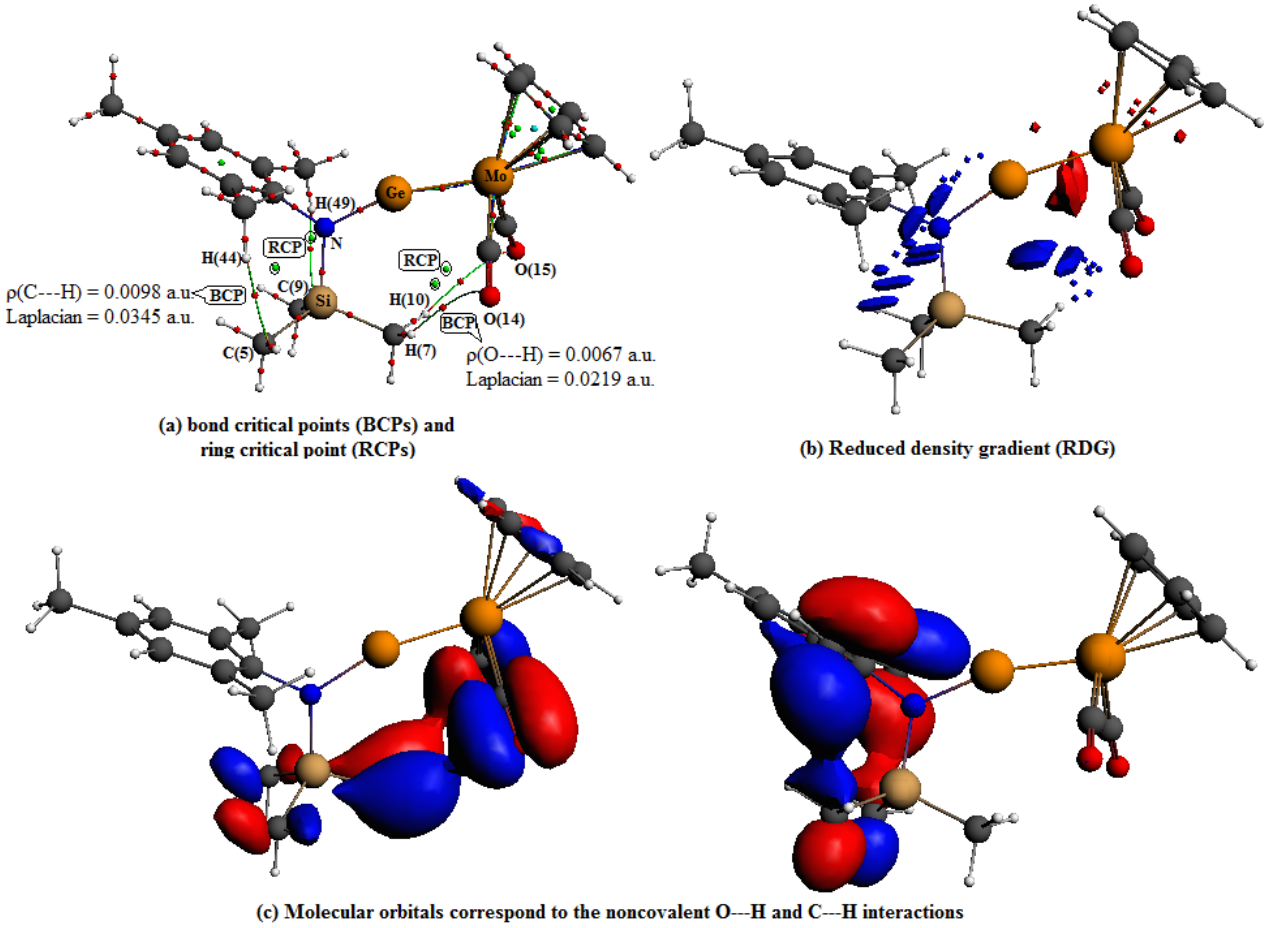

Fig. 7 (**a**) Bond paths, BCPs and RCPs (circled) of the complex [(η^5-C_5H_5)$(CO)_2$Mo≡EN($SiMe_3$)(Mes)] (**IX**), (**b**) plot of the reduced density gradient at low density for non-covalent interactions, and (**c**) important molecular orbitals showing O---H and C---H interactions.

3.3. Dispersion contributions in I – X and energy decomposition analysis: To rationalize the contribution of dispersion interactions in the complexes, **I** - **X** and to compute the reliable M≡E bond dissociation energies (BDEs), we performed single point energy calculations using Grimme's DFT-D3 and DFT-D3(BJ) methods on the structures optimized with density functionals BP86, PBE, PW91 and TPSS. The bond dissociation energies and dispersion-corrected BDEs (BDE + Dis) of the complexes **I** - **X** are collected in Table 4.

Table 4

As can be seen in Table 4, the values of BDEs are depends on the choice of density functionals and follow the order 140.6-175.3 kcal/mol (RPBE) < 145.8-177.6 kcal/mol (BP86) < 147.2-180.8 kcal/mol (PBE) < 147.9-181.2 kcal/mol (PW91). The results reveal that the BDEs without dispersion corrections are largest for PW91among the employed GGA functionals. The non-covalent interactions appear to be a very important contributor to the bond dissociation energy. With the incorporation of the DFT-D3 dispersion corrections, the BDEs are enhanced considerably, ranging from 151.3-185.1 kcal/mol (BP86), 150.6-185.3 kcal/mol (PBE), 151.3-185.9 kcal/mol (PW91) and 151.4-186.3 kcal/mol (TPSS), which further increases with the addition of Becke-Johnson (BJ) damping function (Table 4). Although, the dispersion corrections has rather small effect on the optimized M≡Ge bond distance of the complex **IX** (Table 2), dispersion corrections to the M≡E bond dissociation energies are quite pronounced, ranging from 4.6 kcal/mol to 11.4 kcal/mol.

The bond dissociation energies of complex **X** have been calculated with functionals BP86, PW91 and M06-L. Results are added in Table 4 and compared with BDEs of the complexes [(η^5-C_5H_5)$(CO)_2$Mo≡GeN($SiMe_3$)(Ph)] (**II**) and [(η^5-C_5H_5)$(CO)_2$Mo≡GeN($SiMe_3$)(Mes)](**IX**). Bond dissociation energies (BDEs) of complexes [(η^5-C_5H_5)$(CO)_2$Mo≡GeN($SiMe_3$)(Ph)] (**II**), [(η^5-C_5H_5)$(CO)_2$Mo≡GeN($SiMe_3$)(Mes)](**IX**) and [(η^5-C_5H_5)$(CO)_2$Mo≡GeN($SiMe_3$)(Ar*)](**X**) with density functionals BP86 and PW91 vary in the order **II** > **IX** > **X** which are consistent with the Mo-Ge bond distances . Similar trend in bond dissociation energies of complexes **II**, **IX** and **X** is observed using metaGGA M06-L functional.

Fig. 8 shows that the DFT-D3 and DFT-D3(BJ) corrections to the BDEs strongly depends on the density functional used. The D3-dispersion corrections with zero-damping are in the range 5.6-8.1 kcal/mol (BP86), 3.3-4.6 kcal/mol (PBE), 3.4-4.7 kcal/mol (PW91), and 4.3-5.5 kcal/mol (TPSS),

which are smaller than the corresponding DFT-D3(BJ) corrections with Becke-Johnson damping 10.1-12.0 kcal/mol (BP86), 5.0-6.5 kcal/mol (PBE), 5.2-9.0 kcal/mol (PW91) and 7.0-8.3 kcal/mol (TPSS). Thus, with largest dispersion corrections, the BP86 functional corresponds to the largest values of BDEs. As the bulkiness of the ligands increases, the contribution of the dispersion corrections is also increased; for example, the dispersion energies for the complex **II** are smaller than that of the complex **IX.** The experimental values of the bond dissociation energies are not known and therefore, the accuracy of the calculated BDEs cannot be determined. However, the dispersion corrected DFT (DFT-D3 and DFT-D3(BJ)) methods provide quite accurate estimate of the dispersion energy.[33] Recently, Lugan et al. have pointed out that the high resolution XRD analysis and DFT calculations are very helpful to rationalize the occurrence of weak interligand interactions.[76, 77]

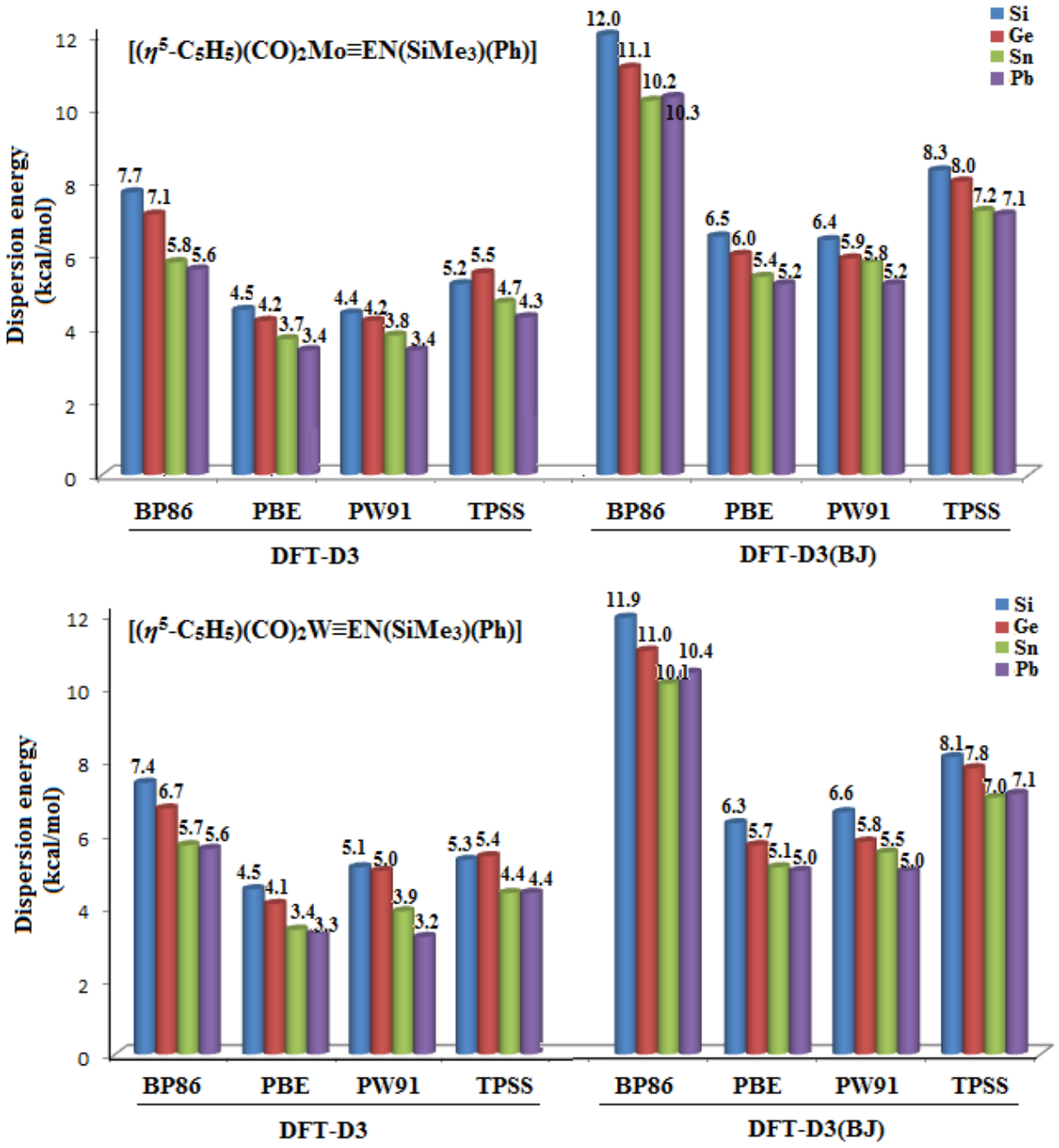

Fig. 8 Trends of dispersion energies in the metal-aminoylyne complexes [(η^5-C_5H_5)$(CO)_2$M≡EN($SiMe_3$)(Ph)] (M = Mo, W; E = Si, Ge, Sn, Pb) (**I – VIII)** as a function of different functionals.

In order to obtain a deeper insight into the nature of the M≡E chemical interactions, we perform the energy decomposition analyses of the complexes **I - IX** considering interaction between

ionic fragments $[(\eta^5\text{-}C_5H_5)(CO)_2M]^-$ and $[EN(SiMe_3)(R)]^+$ in their singlet state as well as interaction between neutral fragments $[(\eta^5\text{-}C_5H_5)\ (CO)_2M]$ and $[EN(SiMe_3)(R)]$ (R = Ph or Mes) in their doublet state (Fig. 1a and 1b, respectively) in C_s symmetry constraint. The various energy terms arising from EDA are collected in Table 5, Table S4 and their trends, from silicon to lead in $[(\eta^5\text{-}C_5H_5)(CO)_2M{\equiv}EN(SiMe_3)(Ph)]$ **I - VIII** are depicted in Fig. 9.

Table 5

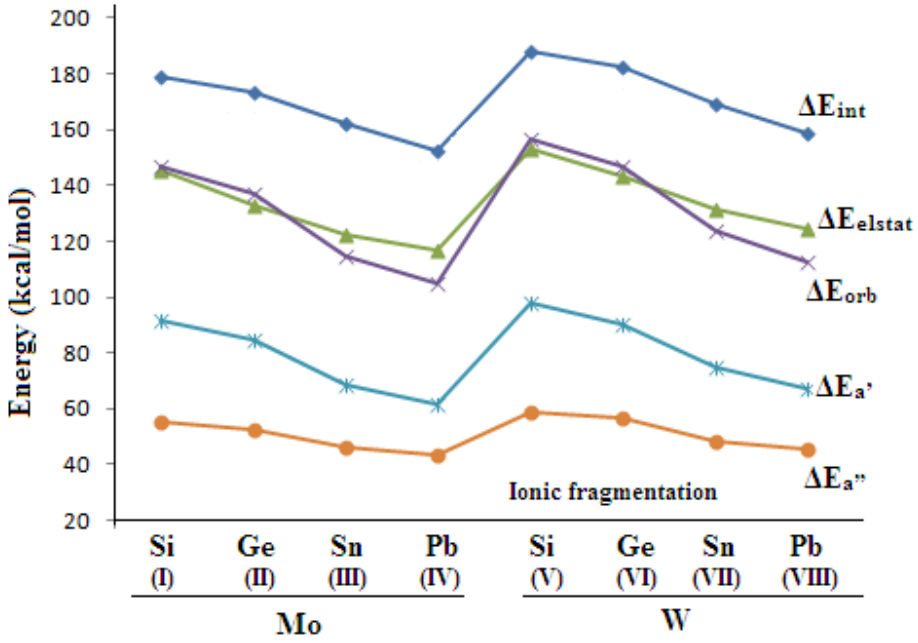

Fig. 9 Trends of various energy terms of the M-E bonds in the metal-aminoylyne complexes $[(\eta^5\text{-}C_5H_5)(CO)_2M{\equiv}EN(SiMe_3)(Ph)]$ (M = Mo, W; E = Si, Ge, Sn, Pb) (**I** – **VIII**) using ionic fragments $[(\eta^5\text{-}C_5H_5)(CO)_2M]^-$ and $[EN(SiMe_3)(Ph)]^+$.

The calculated data in Table 5 (considering ionic fragmentation) show that the interaction energies, ΔE_{int}, are rather high and decreases from silylne to plumbylyne complexes. The tabulated results for tungsten complexes **V**-**VIII** reveal the expected periodic trend in bond strengths due to d-

orbital extent: the W≡E bonds are stronger than the corresponding Mo≡E bonds. The breakdown of the interaction energy, $\Delta E_{int,}$ into the repulsive term (Pauli repulsion, ΔE_{pauli}) and the attractive interactions (ΔE_{orb} and ΔE_{elstat}) shows that the contributions of the electrostatic interactions ΔE_{elstat} and the orbital interactions ΔE_{orb} have almost the same values. Thus, the M≡E bonds have an equal degree of covalent and ionic characters. Fig. 9 shows schematically the variation of the interaction energies (ΔE_{int}) and electrostatic interaction (ΔE_{elstat}), orbital interactions (ΔE_{orb}), ΔE_{σ} and ΔE_{π} of the complexes **I-VIII**. The absolute values of the all energy terms are larger for tungsten complexes than those of the molybdenum complexes and decrease from silylyne to plumbylyne for both set of complexes (Fig. 9). It is important to note that the various energy values of the molybdenum-aminogermylyne complex (**II**) are higher than those of the complex (**IX)**. Table 4 also gives the components of the orbital interaction i.e. contributions of M← E σ-donation and M → E π back-donation. Here, we want to emphasize that the calculated π-energy contribution ΔE_{π} gives the out-of-plane π component of the $[(\eta^5\text{-}C_5H_5)(CO)_2M]^- \rightarrow [EN(SiMe_3)(Ph)]^+$ π back-donation only. This is because the molecules have C_s symmetry and thus orbitals can only have a' (σ) and a" (π) symmetry. Thus, the energy contributions of the a' (σ) orbitals comes not only from the $[(\eta^5\text{-}C_5H_5)(CO)_2M]^- \leftarrow [EN(SiMe_3)(Ph)]^+$ σ-donation but also from the in-plane $[(\eta^5\text{-}C_5H_5)(CO)_2M]^- \rightarrow [EN(SiMe_3)(Ph)]^+$ π back-donation. For the molecules that have only C_s symmetry, it is not possible to separate the later two terms. The energy analysis suggests that, in the complexes **I –VIII,** ~38% of the ΔE_{orb} comes from out-of-plane (a'') π-bonding and thereby, the covalent bonding has a high degree of π character. The M-E σ-bonding contribution is smaller relative to the π-bonding contribution.

The results of energy decomposition analysis considering neutral fragments are presented in Table S4. It reveals that the M≡E interaction energies are significantly small (-70.3 kcal/mol to -103.1 kcal/mol). Values of Pauli repulsive terms, ΔE_{Pauli} are significantly larger for the interaction between

neutral fragments than for the interaction between the charged fragments. The orbital interactions, ΔE_{orb}, are larger than the electrostatic interaction, ΔE_{elstat}, which is contrary to the large charge separation between the interacting fragments (*wide supra*). The contributions of the M≡E π-bonding to the ΔE_{orb} are dramatically larger than the σ- contributions and even in some case of plumbylyne, the values of ΔE_{σ} tends to be repulsive. This is quite misleading because E-N π-bonding would be expected to reduce the M-E π-bonding. All these observations do not justify the M≡E triple bonding picture in aminoylyne complexes. Thus, the donor-acceptor interaction considering ionic fragments $[(\eta^5\text{-}C_5H_5)(CO)_2M]^-$ and $[EN(SiMe_3)(R)]^+$ seems better choice for bonding in the studied aminoylyne complexes.

Table S5 shows the calculated energy values of the M≡ER and M≡ENR_2 bonds in the metal-ylyne complexes of molybdenum and tungsten. The results reveal that the absolute values of the various bonding energy terms between the ionic fragments $[(\eta^5\text{-}C_5H_5)(CO)_2M]^-$ and $[EMe]^+$[33,34] are larger than those between ionic fragments $[(\eta^5\text{-}C_5H_5)(CO)_2M]^-$ and $[EN(SiMe_3)(Ph)]^+$ (M = Mo, W; E = Si, Ge, Sn, Pb). The M≡E bonds are weaker in complexes **I-VIII** due to formation of E-N π-bonding. As depicted in Fig. 1, the nitrogen can donate π-electron density to the heavier E element which results in E-N multiple bonding characters, and reduces the π-acidity of ENR_2 ligands.

4. Conclusions

Here, for the first time, we reported the quantum-chemical studies including dispersion corrections to analyze the nature of the M-$EN(SiMe_3)(R)$ bonds in metal-ylyne complexes of molybdenum and tungsten $[(\eta^5\text{-}C_5H_5)(CO)_2M{\equiv}EN(SiMe_3)(Ph)]$ (M = Mo, W; E = Si, Ge, Sn, Pb), $[(\eta^5\text{-}C_5H_5)(CO)_2Mo{\equiv}GeN(SiMe_3)(Mes)]$ and $[(\eta^5\text{-}C_5H_5)(CO)_2Mo{\equiv}GeN(SiMe_3)(Ar^*)]$. The DFT-D3/TPSS optimized geometry of the complex $[(\eta^5\text{-}C_5H_5)(CO)_2Mo{\equiv}GeN(SiMe_3)(Ar^*)]$ is in good agreement with available experimental values.[24] Performance of the meta-GGA functionals (TPSS

and M06-L) for the geometries of the studied complexes is better than the GGA functionals, BP86, PBE, PW91 and RPBE. The short M≡E bonds and calculated values of Nalewajski-Mrozek bond orders (1.22 – 1.52) indicate the presence of multiple bond character between the transition metal and the heavier group 14 atoms. This work conclusively showed that significant O---H($SiMe_3$) and E---C($SiMe_3$) non-covalent interactions are appeared in aminoylyne complexes, which are characterized by the QTAIM-defined bond paths. The presence of O---H and E---C(O) interactions results the M-E-N bending. In all studied complexes, the net electronic charge is transferred in the direction [M] → [E]. The dispersion interactions enhance the bonding interactions between transition metal fragments [(η^5-C_5H_5)$(CO)_2$M] and ligands [EN($SiMe_3$)(R)], amounting 5.0-12.0 kcal/mol dispersion contribution to the M-E bond dissociation energies. The DFT-D3 dispersion corrections are smaller than the corresponding DFT-D3(BJ) dispersion corrections. With largest dispersion corrections, the BP86 functional corresponds to the largest values of BDEs. The M≡E bonds in the metal-aminoylyne complexes have an almost equal degree of covalent and ionic characters. The contribution of M ← E σ-donation, in all the complexes, is smaller than the M → E π-back donation. The aryl groups (Ph, Mes) do not have noncovalent interaction with Ge atom, while Ge---C($SiMe_3$) and H($SiMe_3$)---O(CO) noncovalent interaction are observed. The aryl substituents on nitrogen have insignificant effect on M-E-N bending. The absolute value of ΔE(HOMO-LUMO) for M06-L functional is significantly smaller than the GGA functionals. The larger noncovalent interaction and smaller absolute values of ΔE with M06-L functional are responsible for lowering the M-E-N bond angle. Bond dissociation energies (BDEs) of complexes **II**, **IX** and **X** with density functionals BP86 and PW91 vary in the order **II** > **IX** > **X**.

5. References

1 R. S. Simons and P. P. Power, *J. Am. Chem. Soc.*, 1996, **118**, 11966-11967.

2 G. Balázs, L. J. Gregoriades and M. Scheer, *Organometallics*, 2007, **26**, 3058-3075.

3 L. Pu, B. Twamley, S. T. Haubrich, M. M. Olmstead, B. V. Mork, R. S. Simons and P. P. Power, *J. Am. Chem. Soc.*, 2000, **122**, 650-656.

4 A. C. Filippou, A. I. Philippopoulos, P. Portius and D.U. Neumann, *Angew. Chem. Int. Ed.*, 2000, **39**, 2778-2781.

5 A. C. Filippou, P. Portius and A. I. Philippopoulos, *Organometallics*, 2002, **21**, 653-661.

6 A. C. Filippou, A. I. Philippopoulos, P. Portius and G. Schnakenburg, *Organometallics*, 2004, **23**, 4503-4515.

7 A. C. Filippou, G. Schnakenburg, A. I. Philippopoulos and N. Weidemann, *Angew. Chem. Int. Ed.*, 2005, **44**, 5979-5985.

8 A. C. Filippou, N. Weidemann, A. I. Philippopoulos and G. Schnakenburg, *Angew. Chem. Int. Ed.*, 2006, **45**, 5987-5991.

9 A. C. Filippou, P. Portius, A. I. Philippopoulos and H. Rohde, *Angew. Chem. Int. Ed.*, 2003, **42**, 445-447.

10 A. C. Filippou, A. I. Philippopoulos and G. Schnakenburg, *Organometallics*, 2003, **22**, 3339-3341.

11 A. C. Filippou, H. Rohde and G. Schnakenburg, *Angew. Chem. Int. Ed.*, 2004, **43**, 2243-2247.

12 A. C. Filippou, N. Weidemann, G. Schnakenburg, H. Rohde and A. I. Philippopoulos, *Angew. Chem. Int. Ed.*, 2004, **43**, 6512-6516.

13 A. C. Filippou, N. Weidemann and G. Schnakenburg, *Angew. Chem. Int. Ed.*, 2008, **47**, 5799-5802.

14 H. Rohde, M. Menzel, F. Renz and A. C. Filippou, *Hyperfine interact*, 2008, **185**, 129-132.

15 B. V. Mork and T. D. Tilley, *Angew. Chem. Int. Ed.*, 2003, **42**, 357-360.

16 A. C. Filippou, O. Chernov, K. W. Stumpf and G. Schnakenburg, *Angew. Chem. Int. Ed.*, 2010, **49**, 3296-3300.

17 A. C. Filippou, O. Chernov and G. Schnakenburg, *Angew. Chem. Int. Ed.*, 2011, **50**, 1122-1126.

18 A. C. Filippou, A. Barandov, G. Schnakenburg, B. Lewall, M. van Gastel and A. Marchanka, *Angew. Chem. Int. Ed.*, 2012, **51**, 789-793.

19 H. Hashimoto, T. Fukuda, H. Tobita, M. Ray and S. Sakaki, *Angew, Chem. Int. Ed.*, 2012, **51**, 2930-2933.

20 A. C. Filippou, B. Baars, O. Chernov, Y. N. Lebedev and G. Schnakenburg, *Angew. Chem. Int. Ed.*, 2013, **52**, DOI: 10.1002/anie.201308433.

21 A.C. Filippou, P. Ghana, U. Chakraborty and G. Schnakenburg, *J. Am. Chem. Soc*., 2013, **135**, 11525-11528.

22 A.C. Filippou, U. Chakraborty and G. Schnakenburg, *Chem. Eur. J.*, 2013, **19**, 5676-5686.

23 P.G. Hayes, Z. Xu, C. Beddie, J.M. Keith, M.B. Hall and T.D. Tilley, *J. Am. Chem. Soc.*, 2013, **135**, 11780-11783.

24 J. Hicks, T. J. Hadlington, C. Schenk, J. Li and C. Jones, *Organometallics*, 2013, **32**, 323-329.

25 K. K. Pandey, M. Lein and G. Frenking, *J. Am. Chem. Soc.*, 2003, **125**, 1660-1668.

26 M. Lein, A. Szabo, A. Kovacs and G. Frenking, *Faraday Soc. Discuss.*, 2003, **124**, 365-378.

27 N. Takagi, K. Yamazaki and S. Nagase, *Bull. Korean Chem. Soc.*, 2003, **24**, 832-836.

28 K. K. Pandey and A. Lledós, *Inorg. Chem.*, 2009, **48**, 2748-2759.

29 K. K. Pandey, P. Patidar and P.P. Power, *Inorg. Chem.*, 2011, **50**, 7080-7089.

30 K. K. Pandey and P. Patidar, *J. Organomet. Chem.*, 2012, **702**, 59-66.

31 K. K. Pandey and P. Patidar, *Polyhedron*, 2012, **37**, 85-93.

32 K. K. Pandey and C. Jones, *Organometallics*, 2013, **32**, 3395-3403.

33 U. Ryde, R. A. Mata and S. Grimme, *Dalton Trans.*, 2011, **40**, 11176-11183.

34 P. Hobza, J. Šponer, and T. Reschel, *J. Comput. Chem.*, 1995, **16**, 1315−1325.

35 A. Tkatchenko, and M. Scheffler, *Phys. Rev. Lett.*, 2009, **102**, 073005.

36 K. E. Riley, M. Pitonák, P. Jurecka, and P. Hobza, *Chem. Rev.*, 2010, **110**, 5023-5063.

37 C. D. Sherill, *J. Chem. Phys.*, 2010, **132**, 110902.

38 O. A. Vydrov and T. van Voorhis, *J. Chem. Phys.*, 2010, **133**, 244103.

39 S. Grimme, *WIREs Comput. Mol. Sci.*, 2011, **1**, 211-228.

40 S. N. Steinmann, and C. Corminboeuf, *J. Chem. Theory Comput.*, 2011, **7**, 3567−3577.

41 S. Grimme, J. Antony, S. Ehrlich and H. Krieg, *J. Chem. Phys.*, 2010, **132**, 154104.

42 (a) A. D. Becke and E. R. Johnson, *J. Chem. Phys.*, 2005, **122**, 154101. (b) E. R. Johnson and A.D. Becke, *J. Chem. Phys.*, 2006, **124**, 174104.

43 S. Grimme, S. Ehrlich and L. Goerigk, *J. Comput. Chem.* 2011, **32**, 1456.

44 J. Klimes and A. Michaelides, *J. Chem. Phys.*, 2012, **137**, 120901.

45 D. Rappoport, N. R. M. Crawford, F. Furche and K. Burke, Approximate Density Functionals: Which Should I Choose? In *Computational Inorganic and Bioinorganic Chemistry*; E. I. Solomon, R. A. Scott and R. B. King, (Eds.); Wiley-VCH: New York, 2009; pp 159-172.

46 (a) A. D. Becke, *Phys. Rev. A*, 1988, **38**, 3098-3100. (b) J. P. Perdew, *Phys. Rev. B*, 1986, **33**, 8822-8824.

47 J. P. Perdew, K. Burke and M. Ernzerhof, *Phys. Rev. Lett.* 1996, **77**, 3865.

48 B. Hammer, L. B. Hansen and J. K. Norskov, *Phys. Rev. B*, 1999, **59**, 7413.

49 J. P. Perdew, J. A. Chevary, S. H. Vosko, K. A. Jackson, M. R. Pederson, D. J. Sing and C. Fiolhais, *Phys. Rev. B*, 1992, **46**, 6671.

50 J. Tao, J. P. Perdew, V. N. Staroerov, G. E. Scuseria, *Phys. Rev. Lett.*, 2003, **91**, 146401.

51 Y. Zhao and D. G. Truhlar, *Acc. Chem. Res.,* 2008, **41**, 157-167.

52 E. van Lenthe, E. J. Baerends and J. G. Snijders, *J. Chem. Phys.*, 1996, **105**, 6505.

53 E. van Lenthe, A. E. Ehlers and E. J. Baerends, *J. Chem. Phys.*, 1999, **110**, 8943.

54 G. te Velde, F. M. Bickelhaupt, S. J. A. van Gisbergen, C. Fonseca Guerra, E. J. Baerends, J. G. Snijders and T. Ziegler, *J. Comput. Chem.*, 2001, **22**, 931.

55 E. J. Baerends, D. E. Ellis and P. Ros, *Chem. Phys.*, 1973, **2**, 41.

56 E. J. Baerends, T. Ziegler, J. Autschbach, D. Bashford, A. Bérces, F. M. Bickelhaupt, C. Bo, P. M. Boerrigter, L. Cavallo, D. P. Chong, L. Deng, R. M. Dickson, D. E. Ellis, M. van Faassen, L. Fan, T. H. Fischer, C. Fonseca Guerra, M. Franchini, A. Ghysels, A. Giammona, S. J. A. van Gisbergen, A. W. Götz, J. A. Groeneveld, O. V. Gritsenko, M. Grüning, S. Gusarov, F. E. Harris, P. van den Hoek, C. R. Jacob, H. Jacobsen, L. Jensen, J. W. Kaminski, G. van Kessel, F. Kootstra, A. Kovalenko, M. V. Krykunov, E. van Lenthe, D. A. McCormack, A. Michalak, M. Mitoraj, S. M. Morton, J. Neugebauer, V. P. Nicu, L. Noodleman, V. P. Osinga, S. Patchkovskii, M. Pavanello, P. H. T. Philipsen, D. Post, C. C. Pye, W. Ravenek, J. I. Rodríguez, P. Ros, P. R. T. Schipper, G. Schreckenbach, J. S. Seldenthuis, M. Seth, J. G. Snijders, M. Solà, M. Swart, D. Swerhone, G. te Velde, P. Vernooijs, L. Versluis, L. Visscher, O. Visser, F. Wang, T. A. Wesolowski, E. M. van Wezenbeek, G. Wiesenekker, S. K. Wolff, T. K. Woo and A. L. Yakovlev, *ADF 2013.01*, Scientific Computing & Modelling NV, The Netherlands.

57 (a) R. F. Nalewajski and J. Mrozek, *Int. J. Quantum Chem.*, 1994, **51**, 187−200. (b) A. Michalak, R. L. DeKock and T. Zeigler, *J. Phys. Chem. A*, 2008, **112**, 7256−7263.

58 C. F. Guerra, J. W. Handgraaf, E. J. Baerends and F. M. Bickelhaupt, *J. Comput. Chem.*, 2004, **25**, 189-204.

59 E. R. Davidson, S. Chakravorty, *Theor. Chem. Phys.*, 1973, **2**, 319-330.

60 E. D. Glendening, C. R. Landis and F. Weinhold, *WIREs Comput. Mol. Sci.*, 2012, **2**, 1-42.

61 J. I. Rodriguez, R. F. W. Bader, P. W. Ayers, C. Michel, A. W. Gotz and C. Bo, *Chem. Phys. Lett.*, 2009, **472**, 149-155.

62 G. Schaftenaar, *MOLDEN5.0*, CAOSCAMM Center, The Netherlands, 1998.

63 F.M. Bickelhaupt and E.J. Baerends, In *Reviews in Computational Chemistry*, K.B. Lipkowitz, D.B. Boyd (Eds), Wiley-VCH, New York 2000, Vol. 15, pp. 1-86.

64 K. Morokuma, *Acc. Chem. Res.*, 1977, **10**, 294-300.

65 T. Ziegler and A. Rauk, *Theor. Chim. Acta*, 1977, **46**, 1-10.

66 T. Ziegler and A. Rauk, *Inorg. Chem.*, 1979, **18**, 1755-1759.

67 M. von Hopffgerten and G. Frenking, *WIREs Comput. Mol. Sci.*, 2012, **2**, 43-62 and references therein.

68 K. K. Pandey, P. Patidar and H. Braunschweig, *Inorg. Chem.*, 2010, **49**, 6994-7000.

69 K. K. Pandey, *Dalton Trans.*, 2012, **41**, 3278-3286.

70 P. Pyykkö and M. Atsumi, *Chem. Eur. J.*, 2009, **15**, 12770-12779.

71 T. A. Albright, J. K. Burdett, M. –H. Whangbo, in *Orbital Interactions in Chemistry*, 2nd Edition, Wiley, New York, 2013, pp136.

72 A. Michalak, R. L. Derock and T. Ziegler, *J. Phys. Chem. A* 2008, **112,** 7256-7263.

73 L. Pauling. *The Nature of the Chemical Bond*, 3rd Ed. Cornell University Press, New York, 1960, p239: The relationship of bond order to length is $d_n=d_1-0.71 \log(n)$ where n is the bond order, d_1 and d_n are the lengths of bonds with bond order 1 and n, respectively.

74 R. G. A. Bone and R. F. W. Bader, *J. Chem. Phys.*, 1996, **100**, 10892-10911.

75 P. Munshi and T. N. G. Row, *J. Phys. Chem. A* 2005, **109**, 659-672.

76 N. Lugan, I. Fernández, R. Brousses, D. A. Valyaev, G. Lavigne and N. A. Ustynyuk, *Dalton Trans.*, 2013, **42**, 898-901.

77 D. A. Valyaev, R. Brousses, N. Lugan, I. Fernández, and M. A. Sierra, *Chem. Eur. J.*, 2011, **17**, 6602-6605.

Table 1 Selected optimized geometrical parameters[a] of the aminoylyne complexes [(η^5-C_5H_5)$(CO)_2$M≡EN($SiMe_3$)(Ph)] (**I** – **VIII**), [(η5-C_5H_5)$(CO)_2$Mo≡GeN($SiMe_3$)(Mes)] (**IX**) and [(η^5-C_5H_5)$(CO)_2$Mo≡GeN($SiMe_3$)(Ar*)] (**X**) using different density functionals.

	BP86			PW91			PBE			RPBE			TPSS			M06-L		
Complex	M-E	E-N	M-E-N	M-E	E-N	M-E-N	M-E	E-N	M-E-N	M-E	E-N	M-E-N	M-E	E-N	M-E-N	M-E	E-N	M-E-N
I	2.247	1.722	167.4	2.242	1.719	167.4	2.245	1.721	167.3	2.254	1.732	166.9	2.232	1.717	177.4	2.207	1.696	170.7
II	2.305	1.845	167.0	2.304	1.839	166.6	2.305	1.842	166.1	2.315	1.856	166.7	2.295	1.837	169.4	2.305	1.827	158.6
III	2.504	2.056	169.5	2.499	2.048	167.0	2.506	2.050	168.9	2.517	2.069	167.0	2.491	2.048	168.4	2.547	2.028	151.2
IV	2.561	2.160	171.8	2.561	2.153	167.5	2.564	2.156	169.1	2.578	2.174	168.4	2.543	2.153	173.2	2.590	2.135	150.8
V	2.252	1.720	175.7	2.249	1.716	173.4	2.250	1.718	174.1	2.258	1.728	174.6	2.244	1.716	173.8	2.227	1.696	166.6
VI	2.303	1.839	175.8	2.304	1.833	171.9	2.307	1.836	171.6	2.312	1.849	175.2	2.293	1.832	175.8	2.308	1.819	162.1
VII	2.503	2.047	173.4	2.502	2.040	171.1	2.506	2.045	171.0	2.516	2.061	171.9	2.493	2.042	172.4	2.534	2.020	155.1
VIII	2.562	2.153	177.1	2.559	2.143	176.0	2.561	2.147	175.5	2.577	2.167	175.8	2.542	2.145	177.0	2.587	2.129	154.5
IX	2.308	1.849	168.4	2.305	1.842	167.6	2.308	1.846	167.4	2.317	1.861	168.4	2.298	1.840	170.4	2.331	1.837	153.0
X	2.315	1.853	159.6	2.310	1.845	159.7	2.313	1.849	159.1	2.320	1.865	162.9	2.300 (2.290)	1.838 (1.832)	163.0 (158.8)[b]	2.313	1.850	156.2
Experimental[c]			2.2811(4)	1.812(2)	155.81(8)													

[a] bond distances are in angstrom (Å) and bond angles are in degree (°). [b] TPSS-D3 geometry. [c] Geometrical parameters for the X-ray characterized complex of [(η^5-C_5H_5)$(CO)_2$Mo≡GeN($SiMe_3$)(Ar*)].[24]

Table 2 Comparison of the structural parameters[a] of molybdenum-aminogermylyne complex [(η^5-C_5H_5)$(CO)_2$Mo≡GeN($SiMe_3$)(Mes)] obtained at DFT, DFT-D3 and DFT-D3(BJ) level of theory.

	Bond distances		Bond angles	Noncovalent distances		
Methods	M–Ge	Ge–N	M–Ge–N	Ge---C(O)	C(5)---H(44)	O---H
DFT/BP86	2.308	1.849	168.4	2.934	2.639	3.019
DFT-D3/BP86	2.303	1.842	163.6	2.907	2.597	2.721
DFT-D3(BJ)/BP86	2.301	1.841	164.6	2.922	2.574	2.786
DFT/PBE	2.308	1.846	167.4	2.914	2.635	2.875
DFT-D3/PBE	2.307	1.845	166.0	2.906	2.625	2.808
DFT-D3(BJ)/PBE	2.304	1.842	165.9	2.911	2.596	2.787
DFT/TPSS	2.298	1.840	170.4	2.954	2.664	3.025
DFT-D3/TPSS	2.290	1.835	166.9	2.920	2.634	2.822
DFT-D3(BJ)/TPSS	2.290	1.833	167.6	2.935	2.612	2.866
Experimental[b]	2.2811(4)	1.812(2)	155.81(8)			

[a] bond distances are in angstrom (Å) and bond angles are in degree (°). [b] geometrical parameters for the X-ray characterized complex of [(η^5-C_5H_5)$(CO)_2$Mo≡GeN($SiMe_3$)(Ar*)].[24]

Table 3 Nalewajski-Mrozek (N-M) bond orders, Hirshfeld charges and Voronoi deformation density (VDD) charges of the complexes [(η^5-C_5H_5)$(CO)_2$M≡EN($SiMe_3$)(Ph)] (M = Mo, W; E = Si – Pb) (**I** – **VIII**), [(η^5-C_5H_5)$(CO)_2$Mo≡GeN($SiMe_3$)(Mes)] (**IX**) and [(η^5-C_5H_5)$(CO)_2$Mo≡GeN($SiMe_3$)(Ar*)](**X**).

	Bond order[a]		Hirshfeld charges				VDD charges			
Complexes	M-E	E-N	M	E	N	[L_nM]	M	E	N	[L_nM]
[(η^5-C_5H_5)$(CO)_2$Mo≡SiN($SiMe_3$)(Ph)] (**I**)	1.43	1.16	0.22	0.19	-0.24	-0.19	0.29	0.10	-0.31	-0.18
[(η^5-C_5H_5)$(CO)_2$Mo≡GeN($SiMe_3$)(Ph)] (**II**)	1.39	1.11	0.23	0.21	-0.24	-0.17	0.28	0.13	-0.31	-0.16
[(η^5-C_5H_5)$(CO)_2$Mo≡SnN($SiMe_3$)(Ph)] (**III**)	1.31	0.99	0.21	0.31	-0.26	-0.20	0.26	0.22	-0.33	-0.20
[(η^5-C_5H_5)$(CO)_2$Mo≡PbN($SiMe_3$)(Ph)] (**IV**)	1.22	0.93	0.21	0.36	-0.27	-0.21	0.25	0.25	-0.35	-0.21
[(η^5-C_5H_5)$(CO)_2$W≡SiN($SiMe_3$)(Ph)] (**V**)	1.52	1.16	0.08	0.22	-0.24	-0.29	0.13	0.12	-0.31	-0.20
[(η^5-C_5H_5)$(CO)_2$W≡GeN($SiMe_3$)(Ph)] (**VI**)	1.48	1.11	0.08	0.24	-0.24	-0.24	0.13	0.14	-0.31	-0.17
[(η^5-C_5H_5)$(CO)_2$W≡SnN($SiMe_3$)(Ph)] (**VII**)	1.38	0.99	0.07	0.33	-0.26	-0.29	0.11	0.22	-0.33	-0.21
[(η^5-C_5H_5)$(CO)_2$W≡PbN($SiMe_3$)(Ph)] (**VIII**)	1.29	0.93	0.07	0.38	-0.27	-0.24	0.10	0.26	-0.34	-0.22
[(η^5-C_5H_5)$(CO)_2$Mo≡GeN($SiMe_3$)(Mes)](**IX**)	1.38	1.10	0.23	0.22	-0.23	-0.18	0.28	0.11	-0.30	-0.18
[(η^5-C_5H_5)$(CO)_2$Mo≡GeN($SiMe_3$)(Ar*)](**X**)	1.35	1.10	0.23	0.23	-0.22	-0.16	0.28	0.13	-0.30	-0.18

[a]E-N bond orders in free ligands are: 1.60 in $[SiN(SiMe_3)(Ph)]^+$, 1.55 in $[GeN(SiMe_3)(Ph)]^+$, 1.37 in $[SnN(SiMe_3)(Ph)]^+$, 1.31 in $[PbN(SiMe_3)(Ph)]^+$, 1.51 in $[GeN(SiMe_3)(Mes)]^+$ and 1.50 in $[GeN(SiMe_3)(Ar^*)]^+$.

Table 4 Bond dissociation energies[a] (BDEs) and dispersion-corrected bond dissociation energies of the M≡E bonds in the complexes [(η^5-C_5H_5)$(CO)_2$M≡EN$(SiMe_3)$(R)] (M = Mo, W; E = Si, Ge, Sn, Pb) (**I-X**) calculating using DFT methods.

Complexes			DFT						DFT-D3				DFT-D3(BJ)			
			BP86	PW91	PBE	RPBE	TPSS	M06-L	BP86	PBE	PW91	TPSS	BP86	PBE	PW91	TPSS
Mo	Si	(**I**)	169.2	173.0	172.5	166.2	171.2	175.9	176.9	177.0	177.4	176.4	181.2	179.0	179.4	179.5
Mo	Ge	(**II**)	163.6	166.8	165.9	159.6	166.2	167.9	170.7	170.1	171.0	171.7	174.7	171.8	172.7	174.2
Mo	Sn	(**III**)	154.6	157.3	156.6	150.2	156.4	149.8	160.3	160.2	161.1	160.9	164.7	162.0	163.1	163.6
Mo	Pb	(**IV**)	145.8	147.9	147.2	140.6	147.1	144.9	151.3	150.6	151.3	151.4	156.1	152.4	153.1	154.2
W	Si	(**V**)	177.6	181.2	180.8	175.3	181.0	186.2	185.1	185.3	185.9	186.3	189.6	187.0	187.8	189.1
W	Ge	(**VI**)	171.7	174.7	173.9	167.7	174.7	176.3	178.4	178.0	178.9	180.1	182.7	179.6	180.5	182.7
W	Sn	(**VII**)	161.6	163.7	163.3	157.3	163.7	158.4	167.3	166.7	167.6	168.1	171.7	168.3	169.2	170.5
W	Pb	(**VIII**)	151.6	153.8	153.1	146.4	152.8	151.8	157.2	156.4	156.9	157.2	162.0	158.1	158.8	159.9
Mo	Si	(**IX**)	158.1	161.1	160.3	153.8	160.6	161.1	166.2	164.9	165.7	166.7	169.8	166.6	167.1	169.0
Mo	Si	(**X**)	148.0	143.9				155.0								

[a]Energies are in kcal/mol.

Table 5 Results of energy decomposition analysis (EDA)[a] of M-E bonds in the complexes [(η^5-C_5H_5)$(CO)_2$M≡EN($SiMe_3$)(Ph)] (M = Mo, W; E = Si – Pb) (**I** – **VIII**) and [(η^5-C_5H_5)$(CO)_2$Mo≡GeN($SiMe_3$)(Mes)] (**IX**) using ionic fragments[b] at BP86/TZ2P level of theory.

Complexes			ΔE_{int}	ΔE_{Pauli}	ΔE_{elstat}[c]	ΔE_{orb}	$\Delta E_{a'}$	$\Delta E_{a''}$ [d]	ΔE_{prep}
Mo	Si	(**I**)	-178.8	113.8	-145.6 (49.8%)	-146.9	-91.5	-55.4 (37.7%)	9.6
Mo	Ge	(**II**)	-173.4	96.6	-132.9 (49.2%)	-137.1	-84.6	-52.5 (38.3%)	9.7
Mo	Sn	(**III**)	-162.1	75.0	-122.5 (51.6%)	-114.7	-68.7	-46.0 (40.1%)	7.6
Mo	Pb	(**IV**)	-152.4	69.5	-117.0 (52.7%)	-104.8	-61.5	-43.3 (41.3%)	6.5
W	Si	(**V**)	-188.1	121.7	-153.3 (49.5%)	-156.5	-98.0	-58.5 (37.4%)	10.5
W	Ge	(**VI**)	-182.7	107.5	-143.2 (49.4%)	-147.0	-90.4	-56.6 (38.5%)	11.0
W	Sn	(**VII**)	-169.4	85.7	-131.5 (51.1%)	-123.6	-75.2	-48.3 (39.1%)	7.8
W	Pb	(**VIII**)	-158.6	78.5	-124.2 (52.4%)	-112.9	-67.3	-45.6 (40.4%)	6.8
Mo	Ge	(**IX**)	-170.8	97.7	-132.5 (49.3%)	-136.0	-84.3	-51.7 (38.0%)	12.7

[a] Energy contributions in kcal/mol. [b] Charged fragments [(η^5-C_5H_5)$(CO)_2$M]$^-$ and [EN($SiMe_3$)(Ph)]$^+$ have been considered. [c]The values in parentheses are the percentage contribution to the total attractive interactions reflecting total ionic character of the bond. [d]The values in the parentheses are the percentage out-of-plane π-character contribution in the total orbital interaction,ΔE_{orb}.

TOC

Assessment of density functionals and paucity of non-covalent interactions in aminoylyne complexes of molybdenum and tungsten [(η^5-C_5H_5)$(CO)_2$M≡EN($SiMe_3$)(R)] (E = Si, Ge, Sn, Pb): A dispersion-corrected DFT study

Krishna K. Pandey,*[a] Pankaj Patidar, Pankaj K. Bariya, Sunil K. Patidar and Ravi Vishwakarma

[a]*School of Chemical Sciences, Devi Ahilya University Indore, Khandwa Road Campus, Indore 452001, India*

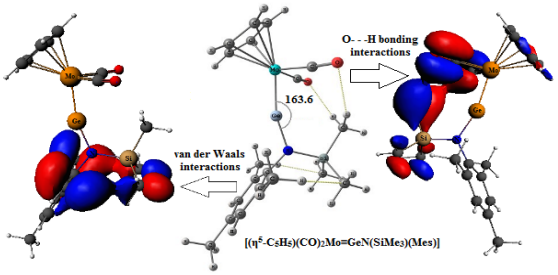

Geometries, bonding analysis and dispersion interactions in aminoylyne complexes of molybdenum and tungsten have been investigated using different density functionals.